

# Detecting object region and working state of aerator based on computer vision and machine learning

Yeqi Liu<sup>1,2,3</sup>, Yingyi Chen<sup>1,2,3,\*</sup>, Huihui Yu<sup>1,2,3</sup>, Xiaomin Fang<sup>1,2,3</sup>, Chuanyang Gong<sup>1,2,3</sup>

1. College of Information and Electrical Engineering, China Agricultural University, Beijing 100083, P.R. China;

2. Key Laboratory of Agricultural Information Acquisition Technology, Ministry of Agriculture, Beijing 100083, P.R. China;

3. Beijing Engineering and Technology Research Center for Internet of Things in Agriculture, Beijing, 100083, P.R. China.

\* Corresponding author(E-mail: [chyinyi@126.com](mailto:chyinyi@126.com)).

## Abstract

Aerator plays an important role in the regulation of dissolved oxygen in aquaculture. The development of computer vision technology provides an opportunity for realizing intelligent monitoring of aerator. Surveillance cameras have been widely used in aquaculture. Therefore, it is of great application value to detect the working state of the aerator with the existing surveillance cameras. In this paper, a method of object region detection and working state detection for aerator is presented. In the object region detection module, this paper proposes a method to detect the candidate region and then determine the object region, which combines the background modeling, the optical flow method and the maximum inter-class interval method. In the work state detection module, this paper proposes a novel method called reference frame Kanade-Lucas-Tomasi (RF-KLT) algorithm, and constructs a classification procedure for the unlabeled time series data. The results of our study show that the accuracy of detecting object region and working state of aerator in the complex background is 100% and 99.9% respectively, and the detection speed is 77-333 frames per second (FPS) according to the different types of surveillance camera. Compared with various foreground detection algorithms and machine learning algorithms, our methods can realize on-line, real-time and high-accuracy detection of the object region and working state of aerator.

**Keywords:** Computer vision; Machine learning; Object region detection; Data analysis; Aerator;

## Highlight

- 1、Object region detection method in complex background is presented.
- 2、A novel method called RF-KLT algorithm for motion state detection in fixed region is proposed.
- 3、Data processing procedure for unlabeled time series data is given.
- 4、Accuracy of detecting object region and working state is 100% and 99.9% respectively, and detection speed is 77-333 FPS.
- 5、The complete solution with existing surveillance cameras for detecting object region and working state of aerator is presented.

## 1. Introduction

Dissolved oxygen is one of the key parameters of water quality in aquaculture. Maintaining the stability of dissolved oxygen content is of great significance for ensuring the safe and rapid growth of aquatic animals and plants (Bardon-Albaret & Saillant, 2016; Chen, Xu, Yu, Zhen, & Li, 2016; Solstorm et al., 2018). As the oxygen increasing equipment with low-cost, high-efficiency, and wide-spread, impeller aerator is often used to ensure the stability of dissolved oxygen. Traditionally, the detection of the working state of aerators mainly depends on human guards or circuit detection (Ma, Zhao, Wang, Chen, & Li, 2015). However, the former method is labor-intensive; and the latter is easily damaged due to the complicated and harsh working environment of aerator. At the same time, the maintenance of the circuit requires professionals to carry out the operation, which is dangerous and difficult to operate. These methods can not find the change of working state timely and accurately.

Computer vision technology is one of the most rapidly developing and mature subfields in artificial intelligence. It has been widely used in various fields to achieve industrialization, such as face recognition (Lu & Tang, 2014), automatic driving (Janai, Güney, Behl, & Geiger, 2017), plant identification (Wäldchen & Mäder, 2018) and so on (Szczypiński, Klepaczko, & Zapotoczny, 2015; Wan, Toudeshki, Tan, & Ehsani, 2018). It is also well used in fisheries management, fish identification and other aquaculture field (Mouy, Rountree, Juanes, & Dosso, 2018). Computer vision technology generally has the characteristics of no human contact, high efficiency and high accuracy. The method based on videos further extends the application scope of computer vision technology. Video frames can not only use a single image processing technology, but also provide more information in the temporal dimension of the inter-frame connection. Computer vision technology based on video images is widely used to detect the change of motion state in traffic monitoring and security field (Jun, Aggarwal, & Gokmen, 2016; Murugan, Jacintha, & Shifani, 2017).

Therefore, the use of existing surveillance cameras and computer vision technology to achieve accurate monitoring of aerator working state without any extra cost, it can reduce labor intensity and detect the change of working state in time, which makes it have great application value. However, there are few studies in this field. (Jinhui He, 2015) proposed a method based on the computer vision technology to use the Harris corner for working state detection between adjacent frames with the detection time of 4 FPS. The real-time performance is not high, and the use of statistical features and discrimination methods are less applicable. Meanwhile, the artificial selection of object region will affect the feature extraction, among which there are many uncertainties. The methodology for robust object region detection and real-time working state detection of aerator using computer vision technology faces two major challenges, which have constrained the development of this methodology.

The first challenge is the complexity of the application scenario, such as differences in the size and angle of the object region, occlusion, ripples, branch shake, camera jitter, dramatic lighting and weather, other water spray and pedestrian interference. The video adds a time dimension to the image, which helps to detect the foreground region (Toyama, Krumm, Brumitt, & Meyers, 1999). The background modeling method can detect a small foreground region (Zivkovic & Ferdinand, 2006), but cannot feedback other features of the foreground region, so it is still difficult to further detect the object region from a large number of candidate foreground regions. Optical flow method has achieved good results in the field of motion detection and target tracking (Arai & Hanazawa, 2009; Lee, Kim, & Lee, 2012; Li, Wu, Matsumoto, & Zhao, 2010). However, the assumptions of the three preconditions of optical flow limit its application scenario, which requires that the motion must confirm the following assumptions: (1)the luminance of the corresponding pixel between adjacent frames is constant; (2)the motion of the corresponding pixel between adjacent frames is slow; and (3)the motion direction of neighboring pixels is similar (Baker & Matthews, 2004). The pyramid method overcomes this obstacle in some extent (BOUGUET, 1999), but it is still impossible to distinguish the temporal and spatial state of the movement from beginning to end.

The second challenge is that it must have some characteristics required by the practical application, such as stable, robust, fast, low-cost, and easy to operate. The deep neural network method performs well in object region detection, object recognition, etc., but the time required to establish the model and the requirements for computing resources are too much. And one of the factors that neural networks have made great progress in computer vision technology is that it avoids artificial image feature selection (Krizhevsky, Sutskever, & Hinton, 2012; W. Shi et al., 2016). Therefore, the extracted features must confirm that: (1) the temporal and spatial state of movement can be distinguished easily; (2) the features of the object region have uniqueness in candidate regions of each frame; (3) the stability is very good in complex scenes. It is also important to construct an appropriate dataset from the feature value and choose a fast and efficient training model, because different application scenarios require a timely update of the model.

To address these aforementioned challenges, this paper proposes an RF-KLT algorithm for robust feature extraction and presents a dimension transformation and data processing method for fast model establishment. The aim of this research is to provide a complete solution for the problem of aerator region and its working state detection based on computer vision technology and machine learning algorithms. The study is conducted in two steps: (1) object region detection. For this purpose,

the procedure of maximum contour region detection, candidate region detection, and object region detection is designed. (2) Working state detection. The feature of each frame is extracted with RF-KLT algorithm, and then the time-series dataset is converted into a two-dimensional dataset. The comparison between multiple foreground detection algorithms and machine learning algorithms shows that the proposed method performs well in both steps. In conclusion, our main contributions are as follows:

- Object region detection method in complex background is presented.
- A novel method called RF-KLT algorithm for motion state detection in fixed region is proposed.
- Data processing procedure for unlabeled time series data is given.
- Accuracy of detecting object region and working state is 100% and 99.9% respectively, and detection speed is 77-333 FPS.
- The complete solution with existing surveillance cameras for detecting object region and working state of aerator is presented.

The rest of this paper

## 2. Materials and methods

For each specific surveillance camera with different heights and distances, experiments are required to train corresponding models. The purpose of object region detection is to detect the aerator region, and the purpose of working state detection is to train the classifier to judge the working state. The module of work state detection extracts features from the object region in the reference frame. The relationship and purpose of each module are shown in Fig. 1, and the details of each module are given in 2.2 and 2.3 sections.

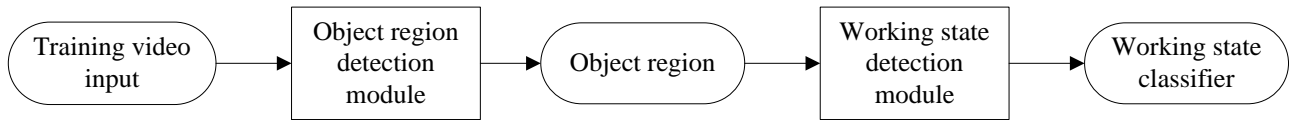


Fig. 1. The relationship and purpose of each module

### 2.1. Video dataset

The video dataset of this article mainly comes from aerator videos within 5 minutes that are extracted in real time by the internet of things (IoT) monitoring platform in Xiongan New Area of China. The presented videos are 8 typical complex scenarios chosen from the video dataset for detecting working state. These videos are from 3 different types of surveillance camera, in which 2 videos are photographed by the camera used to simulate some scenes. The description of video scenes is shown in Table 1. In Table 1, the height of the surveillance camera relative to the object region is divided into three levels: high (H, 8m), medium (M, 5m) and low (L, 2-3m); and the relative distance is also divided into three levels: far (F, >300m), middle (M, 20-70m), and near (N, <15m). It also shows information including time, weather, video parameters, and background description. The video dataset for detecting the object region is the short video clipped in the corresponding video, in which the working state is changed once, and the duration is between 10-20 seconds.

Table 1. Raw dataset description

Video number	Height	Distance	Frame rate (FPS)	Resolution	Weather	Time	Background description
--------------	--------	----------	---------------------	------------	---------	------	------------------------

1	M	M	25	720*1280	overcast	a.m.	Ripple, drainage.
2	M	M	25	720*1280	sun	p.m.	Direct sunlight, surveillance camera automatically set black and white mode.
3	M	M	25	720*1280	overcast	a.m.	Human walking, ripple, drainage.
4	H	M	12	352*640	overcast	p.m.	Occlusion.
5	H	M	12	352*640	overcast	a.m.	Occlusion, human walking.
6	L	N	25	1080*1920	sun	p.m.	Using a camera to simulate a close range scene.
7	L	N	25	1080*1920	overcast	a.m.	Using camera to simulate the strong wind causes camera shake, branch shaking and ripple.
8	H	F	25	352*640	overcast	p.m.	Rocking branch, ripple.

In order to prove the robustness of the model, the pedestrian interference was added to these aerator videos, and the videos were selected under complex scenes such as complicate weathers, different time periods, strong winds, and surveillance camera jitter. Because of the complexity of the working environment, for example, the illumination in practice could change gradually or suddenly, video dataset are also augmented artificially by adding noise and varying brightness in various proportions. The gray change formula is shown in Formula (2-1).

$$p'(x,y) = \begin{cases} p(x,y) + v & (0 \leq p(x,y) + v \leq 255) \\ 0 & (p(x,y) + v < 0) \\ 255 & (p(x,y) + v > 255) \end{cases} \quad (2-1)$$

Where  $p(x, y)$  is the original gray value at the image pixel  $(x, y)$ ,  $v$  is the amount of gray change,  $p'(x,y)$  is the changed gray value at the image pixel  $(x, y)$ . In this study, the augmented video dataset was determined by changing the ratio of gray and noise within twice the area of object region. The random number is used in the ratio change. In Table 2, all augmented datasets are based on video 1, and it also shows the random ratio, step size, signal-noise ratio (SNR), and whether the reference frame makes the same change. For example, for video P3, the gray of the reference frame and current frame in the video is increased by 40 in all rows and all columns of the image pixel, and salt-and-pepper noise with the SNR in the range of [0.01, 0.1] is randomly added with 0.01 step size changing in all rows and columns of the image pixel.

Table 2. Augmented dataset description

Augmented video number	Raw video number	Change ratio of rows(step size is 0.1)	Change ratio of columns(step size is 0.1)	Change range of gray(step size is 1)	SNR of salt and pepper noise(step size is 0.01)	Whether reference frame makes the corresponding change
P1	1	[0:1]	[0:1]	[-80,80]	[0.01,0.1]	Yes
P2	1	[0:1]	[0:1]	+40	[0.01,0.1]	Yes
P3	1	All	All	+40	[0.01,0.1]	Yes

P4	1	All	All	+80	[0.01,0.1]	Yes
----	---	-----	-----	-----	------------	-----



(a) Gray image of object region



(b) Gray value of the front 1/2 rows increases by 80



(c) Gray value of the post 1/3 columns reduces by 30



(d) Random salt and pepper noise in the front 4/5 rows(SNR=0.04)

Fig. 2. Example of artificially augmented dataset

## 2.2. Object region detection

Because the object region determined artificially will lead to the detection of the extra feature points and affect the detection effect, this paper proposes an automatic detection method for the aerator region. The method extracts the integrated features from the motion feature and gray feature in inter-frames, and the contour feature in key frame. This method detects the object region in three steps, which is summarized as the detection of maximum contour regions, candidate regions and object region: (1) an adaptive Gaussian mixture model is used to detect the maximum contour region of each frame; (2) the candidate region is detected from the maximum contour regions by integrating the gray feature in inter-frames and the contour feature in key frame; (3) the object region is detected through the candidate regions by calculating the maximum inter-class interval of the motion features dataset based on RF-KLT algorithm. The flow chart of this section is shown in Fig. 3.

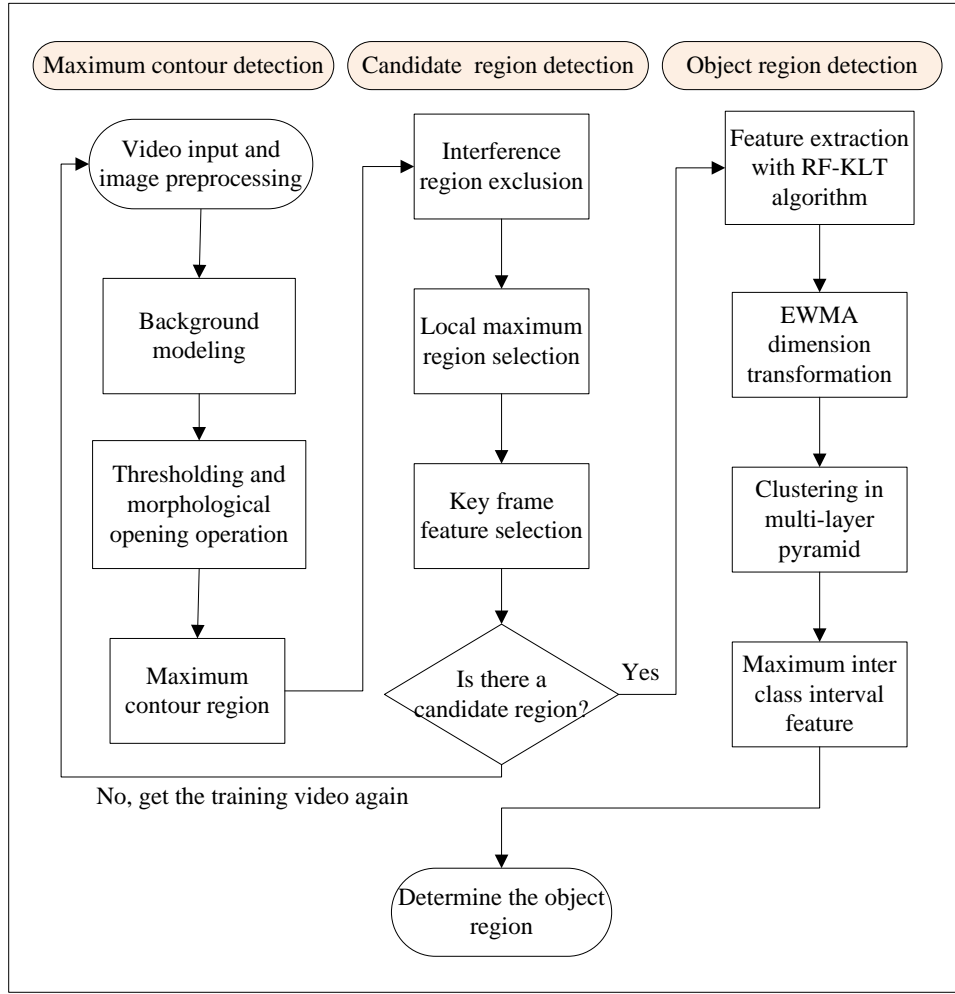


Fig. 3. The algorithm flow of object region detection

### 2.2.1. Maximum contour detection

This research detects the set of maximum contour regions by an adaptive Gaussian mixture model (Zivkovic, 2004; Zivkovic & Ferdinand, 2006). Background is usually a fixed region with less change, and it is usually assumed that the background can be described by a statistical model. The Gaussian mixture model uses multiple weighted and mixed Gaussian models to analysis background characteristics. And the foreground can be detected by marking the part of the image that does not conform to this background model. The Gaussian mixture model (Kaewtrakulpong & Bowden, 2002) can detect the region with small change in the video image, and the adaptive Gaussian mixture model can increase the detection speed and increase the robustness under illumination and ghost regions (Sobral & Vacavant, 2014). The next two steps of the maximum contour region detection are based on the assumption that the aerator region can be detected by an adaptive Gaussian mixture model in the training video.

In this step, Gaussian smoothing is performed on each frame of the video as a preprocessing step firstly. The size of the Gaussian kernel is  $5 \times 5$ . The main purpose of Gaussian smoothing is to avoid detecting some inconspicuous corners. Secondly, an adaptive Gaussian mixture model is used for foreground detection of each frame. It models each pixel with an adaptive number of Gaussian distributions, using the color values of these pixels in the length of the time in the video as a mixed weight, because the color of the background generally lasts the longest and is more static. Thirdly, threshold each frame to obtain a binary image, this research selects a fixed threshold of 240, which can avoid interference in shadowed regions. Fourthly, each

frame is subjected to morphological operations to eliminate small regions and separate more obvious foregrounds. The advantage is to smooth the boundary of the larger object region without significantly changing the area. Finally, contour detections are performed on these foregrounds to obtain a region with the largest area from each frame of the video, which constitutes the set of the maximum contour regions.

### 2.2.2. Candidate region detection

There are too many regions in the set of maximum contour regions, but the areas of the maximum contour regions in most video frames are small. By excluding these interference regions, the training speed of the model can be accelerated and the accuracy will be improved. As shown in Fig. 4, the regularity curve between the areas of the maximum contour region and the number of frames obeys the law shown in Formula (2-2). In maximum contour regions, the first 1/4 regions with the largest area are selected to exclude interference regions with a small area. In order to avoid interference and repeated detection in adjacent regions, regions where the centroid distance of the contour is larger than a threshold are selected from the rest of maximum contour regions. The local maximum region is selected as a candidate region. 1/10 of the minimum value of the video frame resolution is used as the threshold for excluding adjacent regions.

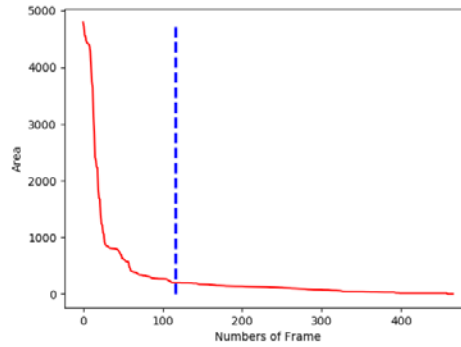


Fig. 4. Example of area distribution of the maximum contour regions

The object region is in two states: the static state and the working state. There are a lot of feature points in both states, because the body of the aerator and the edge of the spray are both changed strongly in the gray value. And the interference region, such as the branch, is also a region of strongly gray change. The features of the single frame image can not detect the characteristics of the object region. The frame that appears in the maximum contour region is selected as a key frame for features extracted of this region. And the first frame of the video when aerator is closed is defined as the reference frame. Compared with maximum contour region in the key frame and corresponding region in the reference frame, features of the gray change in the spray region are extracted. In order to avoid the influence of illumination and improve the detection accuracy of small region, the feature of contour area is considered comprehensively. The feature function of the key frame and the reference frame is determined finally in Formula (2-3).

$$y = \frac{k}{x} (k > 0) \quad (2-2)$$

$$F = \frac{\sum_0^x \sum_0^y (I(x,y) - J(x,y))}{A_{max}} \quad (2-3)$$

Where  $F$  is the feature value extracted in a selected region,  $I(x,y)$  is the gray value of image point  $(x,y)$  in the selected region of the key frame,  $J(x,y)$  is the gray value of image point  $(x,y)$  in the selected region of the reference frame, and

$A_{max}$  is the maximum contour area in the selected region of the key frame. F feature can be used to detect the spray region caused by the work of the aerator, and it is also robust to the monitoring of small object region. If the candidate region is smaller, the area of detected contour is smaller and the corresponding F increases. This paper finally selects the set of regions where the F feature value is larger than the average value in the maximum contour regions as candidate regions.

### 2.2.3. Object region detection

The feature extraction method based on the RF-KLT algorithm and the maximum inter-class interval measurement method both are used to determine the final object region from the candidate regions. In KLT tracker (J. Shi, 1994) and its pyramidal implementation (BOUGUET, 1999), consider an image point  $\mathbf{u} = [x \ y]^T$  on the frame  $I$ . The objective of KLT tracker is to find the location  $\mathbf{v} = \mathbf{u} + \mathbf{d} = [x + d_x \ y + d_y]^T$  on the next frame  $J$  such as the gray value  $I(\mathbf{u})$  and  $J(\mathbf{u})$  are “similar”. The vector  $\mathbf{d} = [d_x \ d_y]^T$  is the optical flow at point  $\mathbf{u}$ . It is essential to define the notion of similarity in a two-dimensional neighborhood sense because of the aperture problem. The optical flow  $\mathbf{d}$  is defined as the vector that minimizes the residual function  $\epsilon$  that defined in Formula (2-4), where the similarity function is measured on an image neighborhood of size  $(2w_x + 1) \times (2w_y + 1)$ . The value of  $w_x$  and  $w_y$  are integers, for which the typical values are 2, 3, 4, 5, 6, 7 pixels.

$$\epsilon(\mathbf{d}) = \epsilon(d_x, d_y) = \sum_{x=u_x-w_x}^{u_x+w_x} \sum_{y=u_y-w_y}^{u_y+w_y} (I(x, y) - J(x + d_x, y + d_y))^2 \quad (2-4)$$

The objective of pyramidal implementation of KLT tracker is also to find the location  $\mathbf{v} = \mathbf{u} + \mathbf{d} = [x + d_x \ y + d_y]^T$  on the next frame  $J$  such as the gray value  $I(\mathbf{u})$  and  $J(\mathbf{u})$  are “similar”, but the point  $\mathbf{v}$  is not in the image neighborhood of size  $(2w_x + 1) \times (2w_y + 1)$ , and is far away from the point  $\mathbf{u}$  in a larger range. It is preferable to have  $d_x \leq w_x$  and  $d_y \leq w_y$  in Formula (2-4) to find the accurate and robust point  $\mathbf{v}$ , so the pyramid is used instead of expanding the size of image neighborhood. The optical flow  $\mathbf{d}^L = [d_x^L \ d_y^L]^T$  at level L in pyramid is defined as the vector that minimizes the new residual function  $\epsilon^L$  that defined in Formula (2-5).

$$\epsilon^L(\mathbf{d}^L) = \epsilon^L(d_x^L, d_y^L) = \sum_{x=u_x^L-w_x}^{u_x^L+w_x} \sum_{y=u_y^L-w_y}^{u_y^L+w_y} (I^L(x, y) - J^L(x + g_x^L + d_x^L, y + g_y^L + d_y^L))^2 \quad (2-5)$$

Where  $\mathbf{g}^L = [g_x^L \ g_y^L]^T$  is available from the computations done from level L to level L + 1 in pyramid, which is computed by Formula (2-6).

$$\mathbf{g}^{L-1} = 2(\mathbf{g}^L + \mathbf{d}^L) \quad (2-6)$$

For level L in pyramid,  $\mathbf{d}^L$  is computed through the same procedure by Formula (2-5), which searches the finest point  $\mathbf{v}$  to minimizes the functional  $\epsilon^L(\mathbf{d}^L)$  in the neighborhood with constant size  $(2w_x + 1) \times (2w_y + 1)$ . This procedure goes on until the bottom level is reached ( $L = 0$ ), and the initial value of the top level ( $L = L_{max}$ ) in pyramid is initialized to zero.

$$\mathbf{g}^{L_{max}} = [0 \ 0]^T \quad (2-7)$$

Therefore, the final optical flow  $\mathbf{d}$  at point  $\mathbf{u}$  is then defined in Formula (2-8).

$$\mathbf{d} = \mathbf{g}^0 + \mathbf{d}^0 = \sum_{L=0}^{L_{max}} 2^L \mathbf{d}^L \quad (2-8)$$

The objective of pyramidal implementation of RF-KLT tracker is the same as the above two methods, but it is changed to find more obvious motion feature, and guarantees the accuracy and robustness of the feature point tracking. For each candidate



region, RF-KLT algorithm proposed in this paper is divided into three steps, the schematic diagram is shown in Fig. 5. (1) Shi-Tomas corner detection method is used to find the corners (point  $\mathbf{u}$ ) of the fixed reference frame. The Shi-Tomas algorithm (Lucas & Kanade, 1981) determines the strong corner point by finding the maximum value from the minimum eigenvalue of each two eigenvalues in the pixel gradient matrix. It can ensure that the number of detected feature points is within a reasonable range, and the feature points in the object region all fall on the body of aerator. (2) Lukas-Kanade algorithm is used to find the matching corners (point  $\mathbf{v}$ ) in current frames corresponded reference frame. The search range of the matching corner points starts from the center of the object region, and the radius of the diagonal of the object region is selected as radius. Lukas-Kanade algorithm instructs how this method is used for feature point tracking and has evolved into a practical KLT

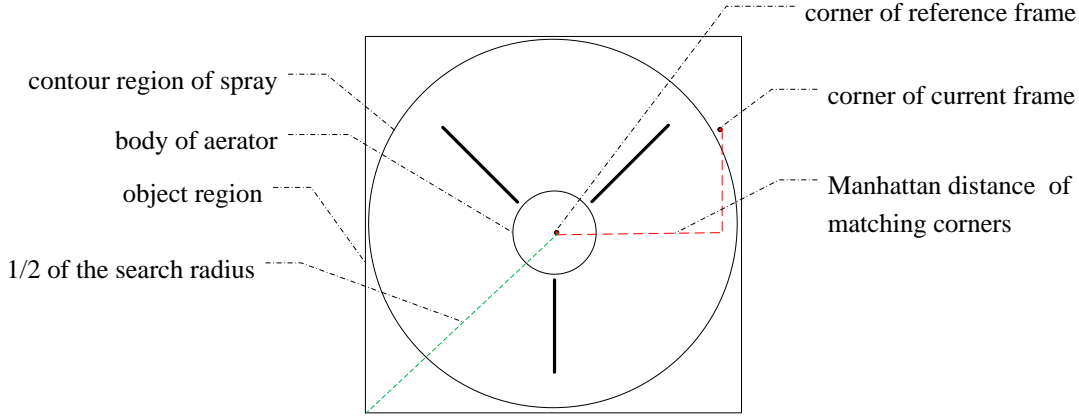


Fig. 5. Dist feature extraction based on RF-KLT algorithm

tracker (J. Shi, 1994). (3) The average distance between matching corners of each frame is extracted as the feature. Manhattan distance is used to measure this distance of the matching corner points. The extraction of Dist features in each frame based on RF-KLT algorithm is shown in Formula (2-11).

$$\epsilon^L(\mathbf{d}^L) = \epsilon^L(d_x^L, d_y^L) = \sum_{x=u_x^L-w_x}^{u_x^L+w_x} \sum_{y=u_y^L-w_y}^{u_y^L+w_y} (I_0^L(x, y) - J^L(x + g_x^L + d_x^L, y + g_y^L + d_y^L))^2 \quad (2-9)$$

$$\mathbf{d} = \mathbf{g}^0 + \mathbf{d}^0 = \sum_{L=0}^{L_{max}} 2^L \mathbf{d}^L \quad (|\mathbf{d}| \leq 2\sqrt{(l/2)^2 + (h/2)^2}) \quad (2-10)$$

Compared with the conventional KLT algorithm, the RF-KLT algorithm is improved in three aspects. The calculation procedure is shown in Formula (2-9) and Formula (2-10), and schematic diagram and result formula as shown in Fig. 5 and Formula (2-11), respectively. Where  $I_0^L(x, y)$  is a point  $\mathbf{u} = (x, y)$  in fixed reference frame in the level  $L$  in pyramid, and  $l$  and  $h$  are respectively the length and width of the candidate region. The main procedure includes: (1) Finding the best matching point of the corresponding corner point in the fixed reference frame, which means that  $I_0^L$  is not changed along with  $J^L$  changed. The goal of this improvement is to obtain the movement state change characteristics with more distinct discrimination, and this is the most critical improvement. (2) Finding the best search radius under the multi-level image pyramid. It means that the range ( $\mathbf{d}$ ) of searching matching point by optical flow method is limited. The goal of this improvement is to ensure that the matching corner is not lost and robust. (3) Using Manhattan distance to measure the distance between the corner points (point  $\mathbf{u}$  and point  $\mathbf{v}$ ), which is also to obtain more obvious movement characteristics. The precondition for matching corners using the optical flow method based on the fixed reference frame is as follows: a multi-level pyramid and a fixed region. These two conditions ensure that the three basic assumptions of the optical flow method are still confirmed.

$$\text{Dist} = \begin{cases} \left(\frac{1}{i}\right) * \sum_0^i |x_{i1} - x_{i0}| + |y_{i1} - y_{i0}| & (0 < i \leq 5) \\ 0 & (i = 0) \end{cases} \quad (2-11)$$

Where Dist is the distance feature value between matching corner points,  $(x_{i0}, y_{i0})$  is the coordinates of the  $i$ -th corner point in the reference frame, and  $(x_{i1}, y_{i1})$  is the coordinates of the  $i$ -th matching corner point in the current frame corresponds to the reference frame.  $i$  is the number of corners. In order to ensure the real-time detection, and according to the number of strong corners on the body of aerator, the most obvious 5 corners with maximum eigenvalue are selected. And  $w_x$  and  $w_y$  are both 7 pixels in this study.

Dist feature is an unlabeled dataset that changes with the number of frames, and it can be considered as sequential data. In order to smooth the data and perform dimensional transformation, the exponentially weighted moving average (EWMA) model (Kim & Chang, 2018) is used to process original dataset, and its calculation formula is shown in Formula (2-12). EWMA model maintains coherence of the inter-frame feature value in a window range. And the most important is that the two-dimensional feature reconstructed by deleting the time dimension is more robust to distinguish. One class of data is close to the origin point, and one class of data is far from the origin point. The two classes of datasets constructed in this way also have good flatness in shape.

$$y_t = \frac{x_t + (1 - \alpha)x_{t-1} + (1 - \alpha)^2x_{t-2} + \dots + (1 - \alpha)^tx_0}{1 + (1 - \alpha) + (1 - \alpha)^2 + \dots + (1 - \alpha)^t} \quad (2-12)$$

Where  $y_t$  is the EWMA feature corresponding to the Dist feature in the current frame;  $x_t$  is the Dist feature in the current frame, which is the Dist feature in the last frame of the sliding window.  $x_{t-1}$  is the Dist feature in the previous frame of the sliding window; ...;  $x_0$  is the Dist feature in the first frame of the sliding window;  $0 < \alpha < 1$ , and  $\alpha = \frac{2}{s+1}$ , where  $s \geq 1$ ,  $s$  is the frame rate of video.  $t$  is the length of the sliding window, and its selection is also automatically obtained based on the frame rate of video.

After data smoothing and dimensional transformation, the dataset has a distinct distribution rule of two classifications. Because the dataset is flat and the numbers of class are known, the K-means clustering method ( $K=2$ ) can accurately obtain the centroid of each class of dataset and thus calculate the inter-class interval feature (Arthur & Vassilvitskii, 2007). Details of K-means clustering method are given in 2.3.2 section. The maximum inter-class interval feature under the multi-level pyramid can prevent the size of the object region from affecting the experimental results. As shown in the Formula (2-13), the region with a largest centFeature is selected as the final object region from the candidate regions. The centFeature under the high level pyramid can avoid a small feature value between two classes in the small region; at the same time, by reducing the proportion of distance features under the high level pyramid, large feature value between two classes in the large region can be avoided.

$$\text{CentFeature} = \sum_0^i \frac{\text{Diff}}{2^i} \quad (0 \leq i \leq 4) \quad (2-13)$$

Where CentFeature is inter-class interval feature of the selected candidate region. Diff is the difference of abscissa values between two class centroids under the  $i$ -th pyramid of the selected region, and  $i$  is the number of pyramid levels, increasing from 0 to 4 levels.

### 2.3. Working state detection

The purpose of this section is to achieve automatic detection of aerator working state. The algorithm flow of working state detection is shown in Fig. 6. In this module, the main procedures include feature extraction, feature dataset construction (including EWMA data processing, dimension transformation), data labelling, and classifier training. The details of RF-KLT algorithm and EWMA model are described in 2.2.3 section. In the reference frame of the RF-KLT algorithm, corner detection is performed in the object region obtained by the module of object region detection.

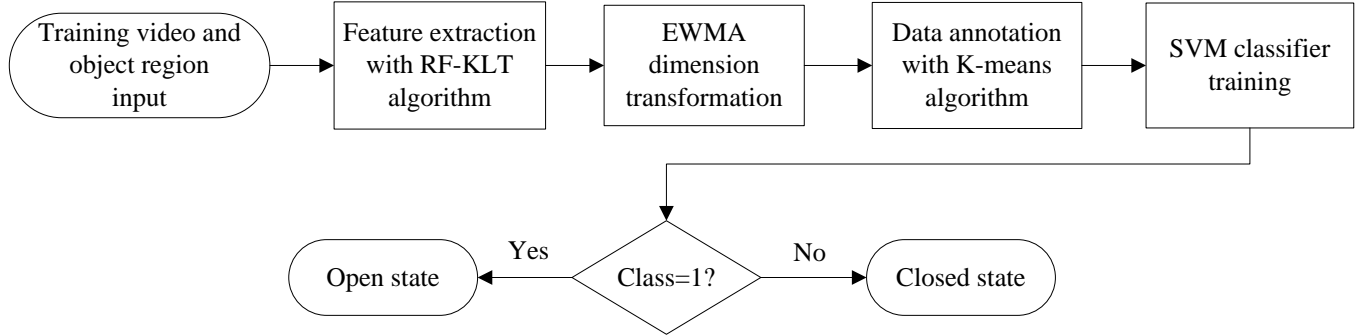


Fig. 6. The algorithm flow of working state detection

#### 2.3.1. Feature extraction and dataset construction

The extraction of image features in computer vision is a very critical step. The purpose of RF-KLT algorithm is to extract robust features for the change of motion state. More importantly, corner matching is done under the 4-level pyramid. The high level pyramid can increase the search range of corner matching, and get larger features of corner distance variation, which increase the discrimination of datasets of two classes. The conventional optical flow method is based on the detection of adjacent frames, but the corner change features are not obvious in the motion state detection of fixed region. The RF-KLT algorithm can be used to extract more obvious characteristics of motion state change in scenes of brightness change and large scale motions. This algorithm can also be used in other conditions to detect motion state change in a fixed region.

The EWMA model is used to transform the time series data into the same dimensionality to construct a dataset that is smoother and more distinguishable, which can avoid the influence of single error on the experimental results, and can also reduce the influence of the data points from working state change process on the experiment. The constructed dataset has flat and highly discriminating features.

#### 2.3.2. Unlabeled data annotation

Clustering algorithm is widely used in the learning of unlabeled samples, which is used to reveal the inherent laws of data and provide a basis for further data analysis. Clustering algorithm is a typical unsupervised learning algorithm, which is mainly used to automatically cluster similar samples into one class. The number of classes and inter-class characteristics of the datasets constructed in this paper are known, including the on and off of two classes of feature data. One class of data is closer to the origin point, and another is far from the origin point. In order to achieve data labeling, and because of the flatness and aggregation shape of dataset distribution, K-means clustering methods are used to annotate data (Arthur & Vassilvitskii, 2007).

The idea of the K-means algorithm is simple. Firstly, the constant K is determined, which means the number of clusters. In this study, K=2. Then the starting point is selected randomly as the centroid. Secondly, measuring the similarity between each sample and the centroid by Euclidean distance, and placing the sample points in the most similar class. Thirdly, recalculating

the centroid of each class and repeating the procedure until the centroid does not change or reach the upper limit of iterations. Finally, the class to which each sample belongs and the centroid of each class are determined.

In this study, label 1 is assigned to the dataset that is far from the origin point corresponding to the open state, and label 0 is assigned to the dataset that is close to the origin point corresponding to the closed state. The feature data in the state change process and the feature data due to the corner matching errors are determined based on the distance from the centroids of the two classes. This enables automatic labeling of unlabeled datasets. In order to avoid classifying high-error data into one class, the feature dataset constructed by the two working states of aerator must be a balanced dataset in training videos. This study sets the ratio of two classes of dataset between 1/5-5. The object region is very small, the change of the feature is also small, and if the corner matching is not stable, the mismatched feature value will be too large. Then the error data becomes a class of data, and the trained classifier cannot correctly detect the open state. Therefore, the balance of training dataset can avoid such errors.

### 2.3.3. Classifier training

Through the feature extraction from different working states, the construction of datasets, and the labeling of unlabeled data, the final dataset is a triple, which includes two-dimensional feature data and their corresponding labels. The SVM algorithm has a complete theoretical basis and good classification ability, and is widely used in the data classification with limited samples (Wu, Lin, & Weng, 2004). This research constructs a dataset that is linearly separable, so the linear SVM algorithm is used to effectively classify the dataset.

At last, the application procedure of our methods is divided into three steps: (1) the corner distance feature (Dist) of real-time frame is extracted according to the matching corner points in the object region of the reference frame; (2) constructing two-dimensional data using the EWMA model; and (3) classifying data according to trained classifiers. If the class is 1, it indicates that the aerator is currently in the working state; and if the class is 0, the aerator currently is in the closed state.

## 3. Results and discussion

### 3.1. Software and algorithm parameter

In this study, the software is programmed in Python 3.6.3 programming language using the Numpy and Pandas scientific computing libraries. Opencv 3.3.1 in python is used for the basic image processing and video analysis (OpenCV, 2017). Scikit-learn 0.19.1 in python is used for machine learning algorithms comparing (Scikit-learn, 2017). The algorithms development and experiments are based on the 64-bit Intel 3<sup>rd</sup>-Generation Core i5 CPU (i5-3230M, 2.60GHz). This is a personal laptop with a common configuration, indicating that the experimental results have a good reference value in the actual monitoring system configuration.

The precision, recall and f1-score are used to evaluate the results of working state detection, and they are defined as Formula (3-1), Formula (3-2) and Formula (3-3).

$$\text{precision} = \frac{tp}{tp + fp} \quad (3 - 1)$$

$$\text{recall} = \frac{tp}{tp + fn} \quad (3 - 2)$$

$$f1 = 2 * \text{presion} * \text{recall} / (\text{precision} + \text{recall}) \quad (3 - 3)$$

Where  $tp$  is the number of correct samples to be classified correctly,  $fp$  is the number of incorrect samples to be classified correctly, and  $fn$  is the number of incorrect samples to be classified incorrectly. In the comparison experiment of the algorithm,

the key parameters and principled literature in the involved algorithms are given in Table 3. Most of these algorithms are from OpenCV library and Scikit-learn library respectively. The specific meaning and details of the parameters in the algorithm refer to the official documentation, and abbreviations of some algorithm are used in later sections.

Table 3. Algorithms and key parameters in the comparison of experiments

Algorithm	Abbreviation	Key parameters in this study	Reference	Document
Support vector machine	SVM	C=1, kernel: linear	(Wu et al., 2004)	
Linear regression	LR	C=1, solver: liblinear	(Schmidt, Roux, & Bach, 2013),	
Linear discriminant analysis	LDA	solver: svd	(Fan, Lei, & Li, 2008)	Scikit-learn, (Scikit-learn, 2017)
K-Nearest Neighbor	KNN	n_neighbors=5, weights: uniform	(Munther, Razif, Abualhaj, Anbar, & Nizam, 2016)	
Classification and regression trees	CART	criterion: gini	B. LI, Friedman, Olshen, & Stone, 1984)	
Naive bayes	NB	priors: None	(He, Zhang, Li, & Wang, 2011)	
K-means clustering	/	n_clusters=2, init: k-means++, max_iter=300	(Arthur & Vassilvitskii, 2007)	
Spectral clustering	/	n_clusters=2, affinity: rbf, gamma=1.0, assign_labels: kmeans	(Luxburg, 2007)	
Agglomerative clustering	/	n_clusters=2, linkage: ward	(Szekely & Rizzo, 2005)	
Adjacent frame difference	AFD	Gaussian smoothness(kernel: 5*5), threshold of binary image:25	/	
White region selection in HSV space	WRS-HSV	Gaussian smoothness(kernel: 5*5), H: 0-180, S: 0-30, V: 220-255	/	/
Fixed background subtraction	FBS	Gaussian smoothness(kernel: 5*5), threshold of binary image: 25	/	
Gaussian mixture background model	GMB	Gaussian smoothness(kernel: 5*5), threshold of binary image: 240	(Kaewtrakulpong & Bowden, 2002)	

K-Nearest Neighbor algorithm	KNN-B	history=30, Gaussian smoothness(kernel: 5*5), threshold of binary image: 240	(Zivkovic & Ferdinand, 2006)	Opencv, (OpenCV, 2017)
Adaptive Gaussian mixture background model	AGMB	Gaussian smoothness(kernel: 5*5), threshold of binary image: 240	(Zivkovic, 2004; Zivkovic & Ferdinand, 2006)	

### 3.2. Comparison of experiments

#### 3.2.1. Comparison of experiments in the RF-KLT algorithm

Compared with the conventional KLT algorithm, the RF-KLT algorithm proposed in this paper has a significant degree of discrimination of the motion feature in the fixed object region. The comparison of the differences in the change of motion state between the two methods is shown in Fig. 7. For the video with same work state change, the feature change of the reference frame is more obvious than that of the adjacent frame. KLT algorithm has continuous corner motion, and its feature change between matching corner points is small and the degree of distinction is not high. But in the RF-KLT algorithm, the corners in the reference frame are fixed. When the state is unchanged, the matching corner point is itself; and when the state changes, there is no matching corner point in the spray region. The matching corners will follow the dividing line between the spray and the calm water surface. When the spray region is stable in the maximum region, the matching corner position is fixed. Therefore, Dist feature based on the RF-KLT algorithm have a good degree of discrimination on the change of motion state. This method can be also applied to the motion state change detection of other scenes. At the same time, the RF-KLT algorithm selects the Shi-Tomas corner with the largest eigenvalue, and it has a fast speed of 0.002 FPS in video 1 compared to the Harris corner point (Harris, 1988).

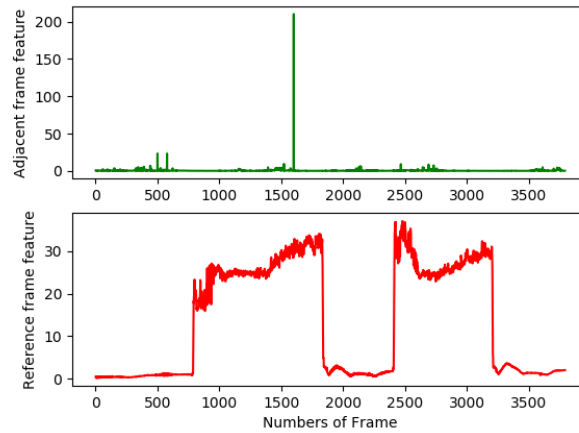


Fig. 7. Comparison of Dist value between conventional KLT algorithm and RF-KLT algorithm (video 1)

RF-KLT algorithm is built on the multi-level pyramid. The relationship between the number of pyramid levels and the distance feature between matching corner points is shown in Fig. 8. In Fig. 8, when the pyramid is higher than four levels, the distinguishability of the characteristics no longer increases. Therefore, the RF-KLT algorithm in the module of working state detection is to match the corner points under the 4-level pyramid. The detection time of each frame and the degree of instability of corner matching increase with the increase of the number of pyramid levels, so higher-level pyramid do not need to be

constructed without improving feature discrimination.

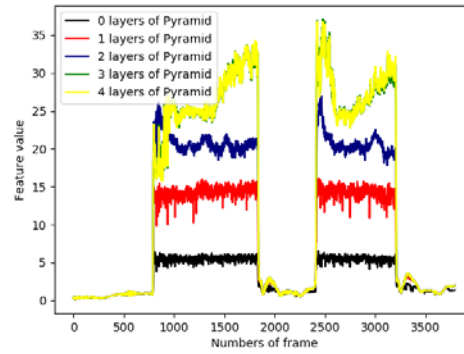


Fig. 8. Comparison of Dist value in different pyramid levels (video 1)

The selection of the reference frame leads to an obvious distinction of the extracted features, so the determination of the reference frame is very critical. The reference frame of the RF-KLT algorithm can be determined in one frame, that is, any frame of the closed state of the aerator can be selected. Fig. 9 shows the accuracy of working state detection with different reference frame in video 1. The experimental results show that there is no effect on the experimental results to select 1<sup>st</sup>, 10<sup>th</sup>, 20<sup>th</sup>, 40<sup>th</sup> or 80<sup>th</sup> frame as the reference frame, which proves that the RF-KLT algorithm is stable and robust.

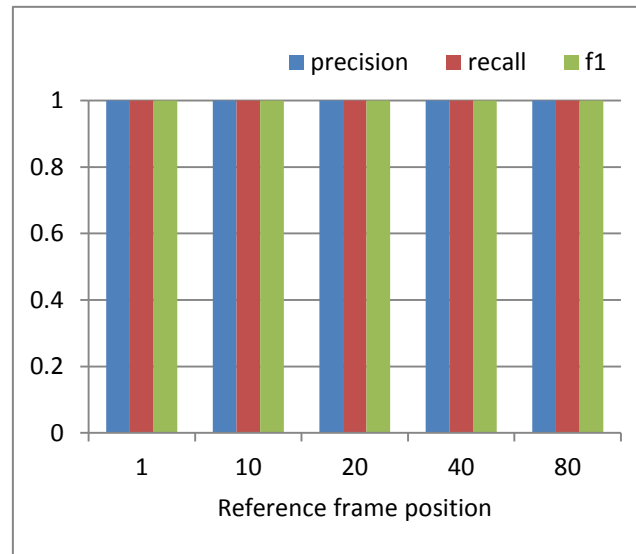


Fig. 9. Comparison of the influence of different reference frame in working state detection module

### 3.2.2. Comparison of foreground detection algorithms

The object region detection of videos in this study is divided into three steps. Table 4 shows the influence of the different foreground detection method on the final detection result in different video datasets. The foreground detection algorithm is used in the maximum contour region detection module, and the subsequent two-step detection methods are not changed. This paper compares the influence of AFD, WRS-HSV, FBS, GMB, KNN-B and AGMB (details in Table 3) on the experimental results in the maximum contour regions detection, and the last method is our selected algorithm. In Table 4, the object region is correctly identified in various complex scenarios based on the KNN algorithm and our model, which shows that the principle of regional selection procedure constructed in this paper is completely correct. For simple background, most algorithms can

accurately detect the object region. However, in complex background, such as the object region is too small or the interference is heavy, the KNN algorithm and our algorithm have good stability. In the time performance of each frame, as shown in Fig. 10, our method is faster than KNN in all scenarios.

Table 4. Comparison of different foreground detection algorithms on experimental results

Video number	AFD	WRS-HSV	FBS	GMB	KNN-B	AGMB(Ours)
1	☑		☑	☑	☑	☑
2	☑	☑	☑	☑	☑	☑
3	☑	☑			☑	☑
4		☑	☑	☑	☑	☑
5	☑		☑	☑	☑	☑
6	☑	☑	☑	☑	☑	☑
7	☑	⊙	☑	☑	☑	☑
8	⊙	⊙	⊙	⊙	☑	☑

(☑ indicates that the final result of object region detection is accurate; ⊙ indicates that the final result of object region detection is inaccurate, but the object region is detected in the candidate regions; and empty table indicates that object region is not detected in the maximum contour regions.)

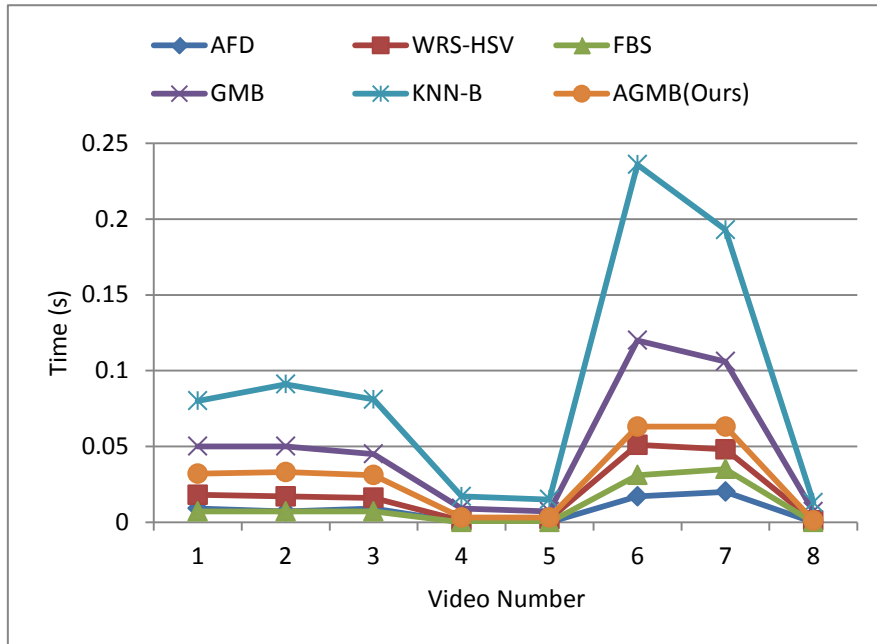


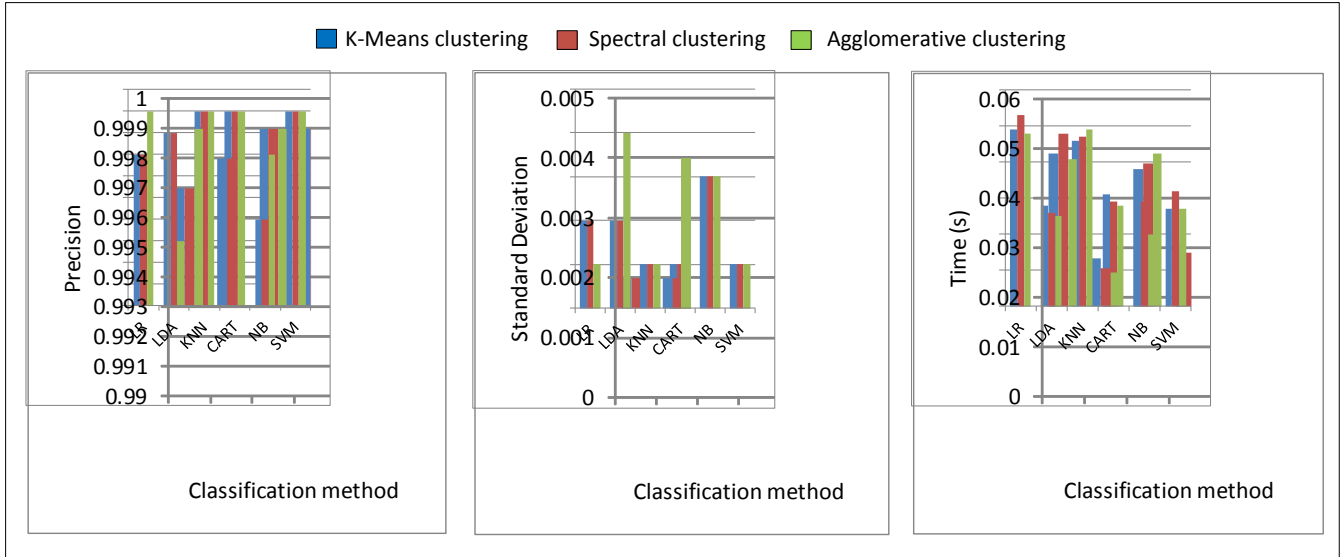
Fig. 10. Speed comparison of different foreground detection algorithms

### 3.2.3. Comparison of machine learning algorithms

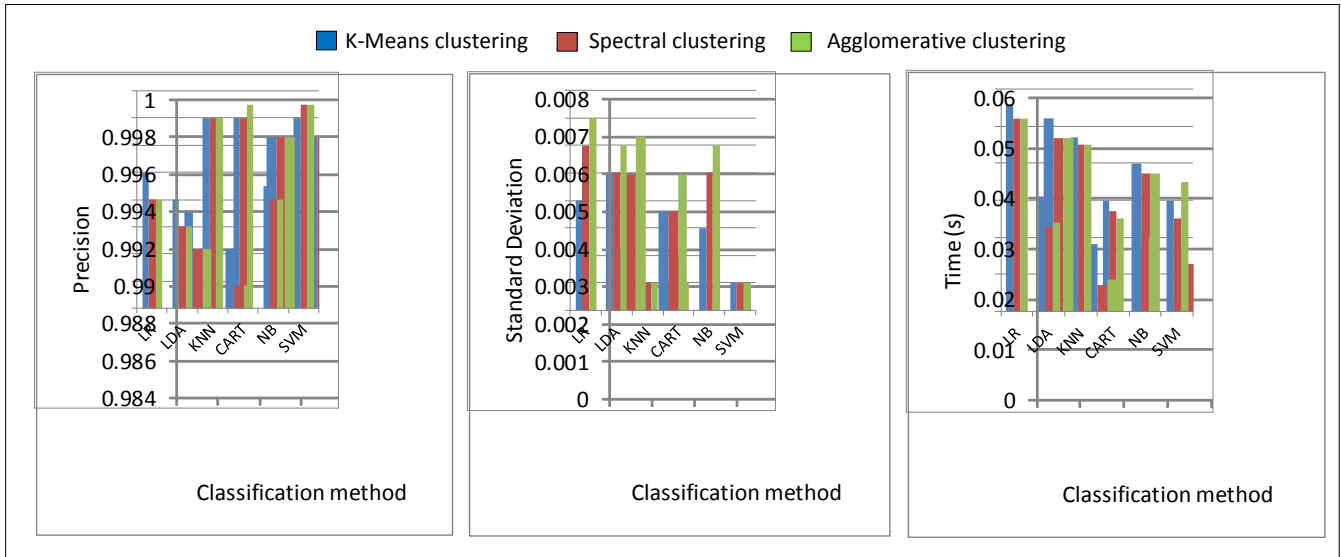
After the data is labelled by the clustering algorithm, a classifier with high precision and high generalization ability can be trained for detecting the working state. The result of the combination of several clustering algorithms and classification



algorithms in video 1 and video 8, which represents simple and complex scenes respectively, is shown in Fig. 11. In this paper, 4/5 of dataset is used as training dataset, and the rest of dataset is used as test dataset. The average precision and standard deviation of the training dataset classification result are determined using a 10-fold cross validation method. In Fig. 11, K-means clustering, spectral clustering and agglomerative clustering with ward linkage are used to label data. LR, LDA, KNN, CART, NB and SVM with linear kernel (details in Table 3) are used to build the classifier for the annotated dataset.



(a) Comparison of different machine learning algorithm combinations in video 1



(b) Comparison of different machine learning algorithm combinations in video 8

Fig. 11. Comparison of different machine learning algorithm combinations in typical video dataset

The principle of selecting a clustering algorithm is based on the regularity of dataset: (1) two classes, (2) linear separation and obvious boundaries between classes, and (3) determination of the class labels corresponding to the different working state of the aerator. Other clustering algorithms such as density clustering algorithms label data into multiple classes because the number of classes cannot be preset. This study compares three linear classifiers: LR, LDA, and SVM with linear kernel. At the same time, three nonlinear classification algorithms have been added for comparison. From the clustering result of video 1 in Fig. 11(a), there are no obvious differences in the three methods of the result in the clustering algorithm; and in the classification algorithm, the accuracy and standard deviation of KNN, CART, and SVM algorithms are all good. However, the

KNN algorithm is worse in time cost, and the CART algorithm is also slightly slower than the SVM algorithm. As shown in Fig. 11(b), for the complex dataset such as the small object region in video 8, the SVM algorithm is also an optimal algorithm in accuracy, standard deviation, and time.

The average time performance of each frame used in the clustering algorithm is shown in Fig. 12. The time performance of the K-means algorithm is one or two orders of magnitude faster than the other two clustering algorithms. According to the accuracy and time analysis, this paper selects the K-means algorithm for data annotation, and selects the linear SVM algorithm to train the classifier. At the same time, the results of algorithm comparison also show the robustness and stability of the feature extraction method and dataset reconstruction method in this study, because the accuracy of dataset classification closed to 100% in the combination of all the different machine learning algorithms. And the accuracy of our algorithm combination in training dataset is 99.9%.

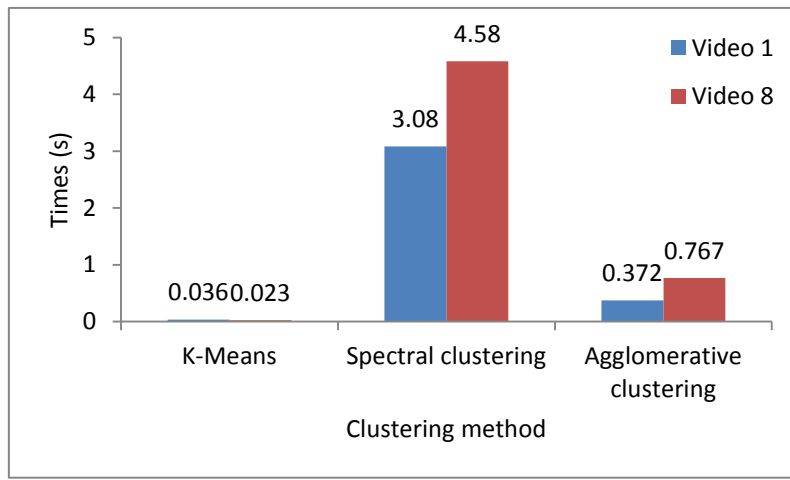


Fig. 12. Speed comparison of different clustering algorithms

As shown in Formula (3-4), in order to avoid labeling the error data as one class, and to prove that the two classes of data labeled by clustering algorithms are closed state and open state respectively, this paper designs a kind of evaluation index—class coefficient (CR), according to the Jaccard coefficient, to measure whether the data is correctly labeled.

$$CR = \frac{|N_{negative} - N_{openframe}|}{N_{frames}} \quad (3 - 4)$$

Where  $N_{negative}$  is the number of negative samples, that is, the number of samples near the zero point;  $N_{openframe}$  is the frame number when the object region is detected in the training video;  $N_{frames}$  is the total number of frames in training video. The CR coefficient is calculated based on working state changed once. It can measure the proportion of a correct sample in the total sample. When it is detected that the frame of the object region appears, that is, the aerator has been opened steadily, the sample data is converted to positive class, thereby the value of  $N_{negative}$  is determined. The degree to which the CR is close to zero indicates how accurately the construction dataset was labeled. However, CR cannot be 0. Because  $N_{openframe}$  is determined when the object region is detected, the matching corner distance feature has reached its maximum value. Some of the samples in the state change process have been classified as positive class. Table 5 is the CR value of video 1 and video 8 corresponding to the above comparison experiment of machine learning algorithms, in which the dataset of the video 8 only cuts one band. The result shows that the clustering methods of this paper have higher accuracy in labeling samples.

Table 5. CR coefficients of different clustering algorithms

CR
----

video number	K-means	Spectral clustering	Agglomerative clustering
1	0.023	0.023	0.023
8	0.059	0.059	0.059

### 3.3. The performance of our methods on object region detection and working state detection

#### 3.3.1. Object region detection

In Fig. 13, the time of each step in the object region detection module and the accuracy of our algorithm in the test dataset are shown. Time1 is the detection time of each frame in maximum contour region detection step, time2 is the detection time of each frame in candidate regions detection step, and time3 is the detection time of each region in object region detection step. The detection of the maximum contour region takes less time, and the time for screening out the candidate object region is even more negligible. This is because the value of gray change in the F feature of object region is calculated along with the contour area, so this step is only judging result. The proportion of the time taken to obtain the largest inter-class interval under the multi-level pyramid is large, which is why the author suggested that the training video of the object region detection module be between 10-20 seconds. And another reason is, as the number of training video frames increases, the number of candidate regions increases accordingly, resulting in an increase in the time for determining the final object region from the candidate regions.

The object region detection is mainly to prepare for the detection of work state. The most crucial step in the feature extraction of work state detection is the matching of corner points. The best result is that all detection corners fall on the body of aerator. In this paper, the detection performance is evaluated according to Formula (3-1). However,  $tp$  is the corner point in object region that is correctly detected and  $fp$  is the corner point in object region that was detected incorrectly. As shown in Fig. 11, the object region is fully detectable according to the precision result.

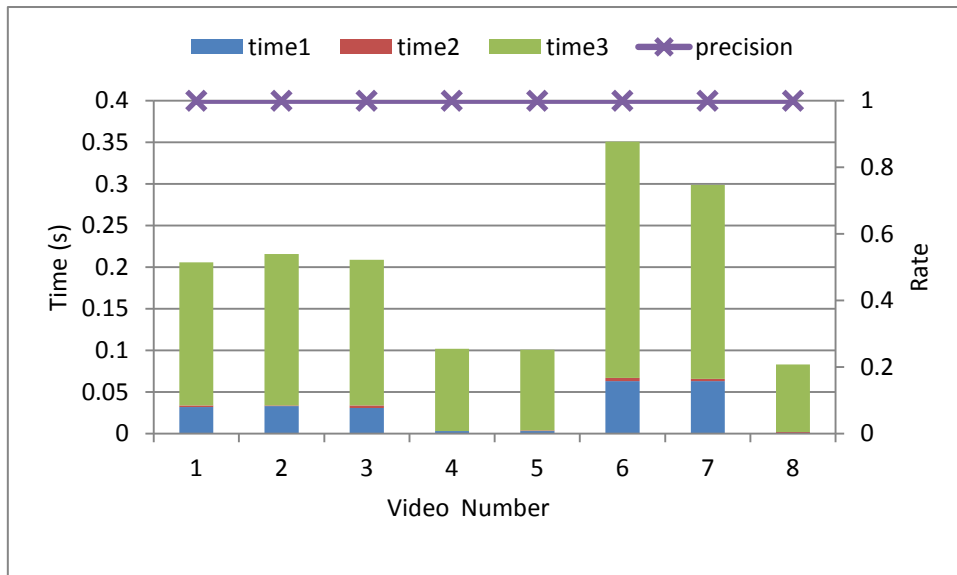


Fig. 13. Time and accuracy of object region detection method for different video datasets

### 3.3.2. Working state detection

The evaluation indicators, including precision, recall and f1-score, of the working state detection in the video datasets are shown in Fig. 14, and the detection time of each frame is shown in Fig. 15. In Fig. 14, the discriminant model can reach 100% accuracy in test dataset in all scenes that include videos with artificially increasing brightness and noise. This results mean that the features extracted based on the RF-KLT algorithm, the method of datasets constructed, and labeling method are all robust. In Fig. 15, videos 6 and 7 are camera supplement scenes. Due to its highest resolution, the detection time of each frame is longer. The detection time from different types of surveillance cameras is different and the detection time increases with the higher resolution of the surveillance camera. The results show that the detection speed of real surveillance cameras is between 77-333 FPS, which is much higher than 25 FPS of surveillance cameras. This method is robust and real-time in many complex scenarios. At the same time, the results of the augmented video dataset artificially prove the stability of the method.

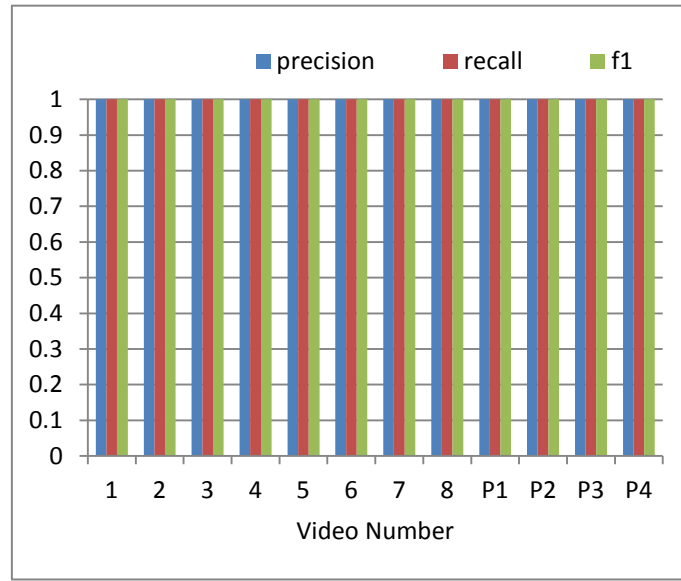


Fig. 14. Performance of working state detection for different video datasets

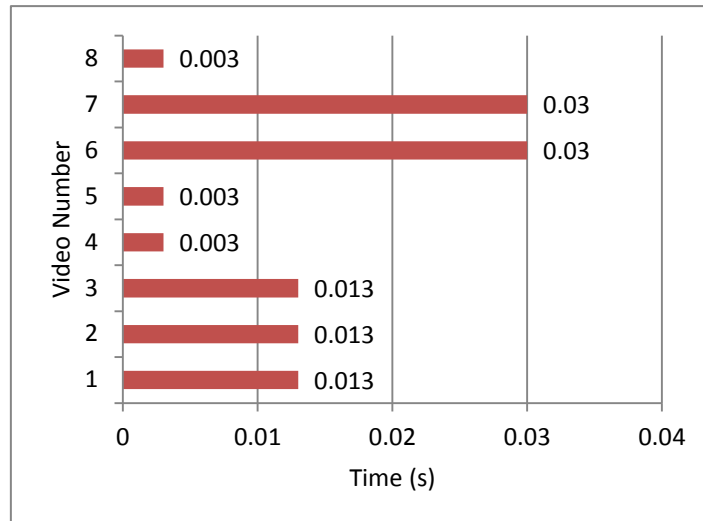


Fig.15. Time of working state detection for different video datasets

The result of object region detection, feature extraction, and EWMA data processing, data labelling, and classification in the algorithm flow of this paper are shown in Fig. 16. Fig. 16(c) shows that the detection of the object region by our method is

accurate. Fig. 16(d) shows that features extracted based on the RF-KLT algorithm have very distinct discrimination and stability under various scenarios. After the K-means clustering method labels the data, the support vectors of the SVM algorithm are all in the process of the working state change, that is, the feature vector from the beginning of the spray to reach the maximum region. There is a clear separation between the two classes of dataset in Fig. 16(e).

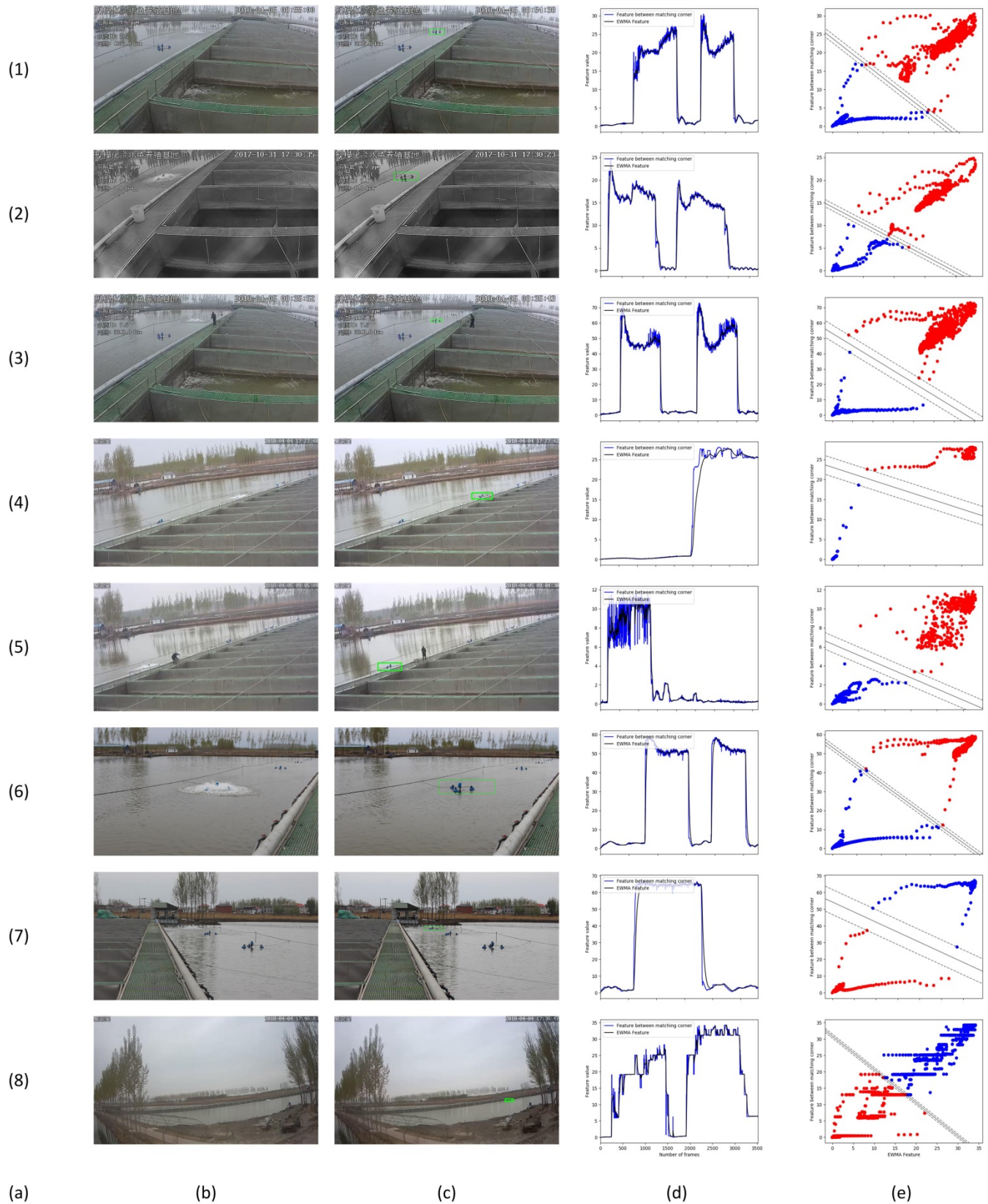




Fig. 16. The result of key algorithm flow in video dataset: (a) is the video number, (b) is a frame of the opening state of the aerator in video dataset. (c) is the result of the object region detection. (d) is the feature curve based on the RF-KLT algorithm and the data after EWMA processing, and (e) is the result of dataset construction, data annotation and classification.

However, in a very small object region, because the number of detected corner points is small and the area of the spray region is small, resulting in a smaller corner distance feature. Therefore, the discrimination of datasets is not obvious. Fig. 17 shows the some results in algorithm flow for P1-P4, which are video datasets with artificially augmented interference. The results show that the influence of brightness is greater than that of noise, and the randomly changed brightness does not affect the experimental results. A non-skipping increase in brightness does not affect the detection results, and even better situations may occur. But when the amount of brightness change is extreme and constant, the instability of the feature data is increased. This is because when the brightness of the object region changes sharply, the corner points detection based on the feature value of gray variation will change, resulting in a change of the distance features between matching corners.

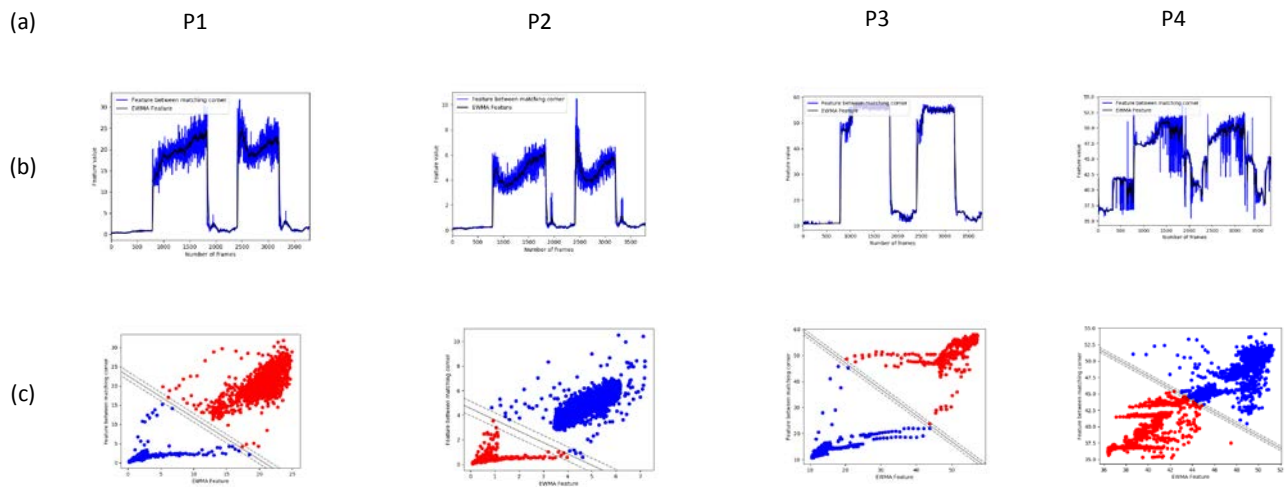


Fig. 17. The result of key algorithm flow in the artificially augmented dataset: (a) is the video number, (b) is the feature curve based on the RF-KLT algorithm and the data after EWMA processing, and (c) is the result of dataset construction, data annotation and classification. The artificially augmented video dataset is based on video 1, so the object region is the same as the object region in video 1.

### 3.4. Suggestions and future work

Based on practical applications and the problem of intense change in brightness, the author suggests: (1)in order to avoid the influence of drastic change in the light intensity in different seasons or time periods, light sensors can be used to measure the dramatic change in light and the classifier model is updated accordingly. The author suggests updating the classifier when the steady increase of gray value reaches 80. (2)Feature is extracted every 5 seconds, and the working state is classified by combining multiple consecutive results in scenes of light strongly changed. (3)The working state detection algorithm in this paper can use a single surveillance camera to monitor multiple aerator regions at the same time, but the object region detection module needs to be revised.

This study was based on video dataset during the day and could not be monitored at night unless lighting equipment with high power was used, but this is a waste of energy. Hence, authors expect to use surveillance cameras with infrared night vision equipment or other night vision equipment for imaging and analysis.

#### 4. Conclusions

This article proposes a method for fast and accurate detection of the aerator object region and working state with existing monitoring equipment. Focusing on the complex working background of the aerator and the heavy interference, and the requirements of stability, accuracy, and real-time in the application, (1) this paper proposes an RF-KLT algorithm for extracting the stable motion features of the fixed region. The novel algorithm extends the applicability of the conventional optical flow method and breaks the limitation of adjacent frames. (2) This paper studies the characteristics of the change of the water spray in video, and constructs the algorithm flow for object region detection, including maximum contour region detection, candidate region detection, and object region detection. The flow of object region detection is suitable for screening the foreground region in a complex background. (3) This paper presents a dimension transformation method for unlabeled time series data. The feasibility of the dataset construction method was proved in various machine learning algorithms. And the experimental results show that the accuracy of object region detection is 100%, the average accuracy of working state detection is 99.9%, and the detection speed is between 77-333 FPS according to different surveillance cameras. This method can realize zero-cost, high-accuracy and real-time aerator object region detection and working state detection, providing a complete solution for the timely regulation of dissolved oxygen and other water quality parameters in aquaculture.

#### Acknowledgments

This research is supported by the Science & Technology Program of Beijing “Research and Demonstration of technologies equipment capable of intelligent control for large-scale healthy cultivation of freshwater fish”(No. Z171100001517016), and the Shandong Province key Research & Development Program “Research and Demonstration of accurate monitoring and controlling technologies for environment of vegetable in facility”(No.2017CXGC0201).

#### References

- Arai, K., & Hanazawa, A. (2009). Detection of optical flow based on local motion signals detected by spatiotemporal Gabor filter. *Neuroscience Research*, 65(Suppl1), S110-S110.
- Arthur, D., & Vassilvitskii, S. (2007). *k-means++:the advantages of careful seeding*. Paper presented at the Eighteenth Acm-Siam Symposium on Discrete Algorithms, New Orleans, Louisiana.
- Baker, S., & Matthews, I. (2004). Lucas-Kanade 20 Years On: A Unifying Framework. *International Journal of Computer Vision*, 56(3), 221-255.
- Bardon-Albaret, A., & Saillant, E. A. (2016). Effects of hypoxia and elevated ammonia concentration on the viability of red snapper embryos and early larvae. *Aquaculture*, 459, 148-155.
- BOUGUET, J.-Y. (1999). Pyramidal implementation of the Lucas Kanade feature tracker description of the algorithm. *Opencl Documents*, 22(2), 363-381.
- Chen, Y., Xu, J., Yu, H., Zhen, Z., & Li, D. (2016). Three-Dimensional Short-Term Prediction Model of Dissolved Oxygen Content Based on PSO-BPANN Algorithm Coupled with Kriging Interpolation. *Mathematical Problems in Engineering*, 2016, (2016-4-24), 2016, 1-10.
- Fan, B., Lei, Z., & Li, S. Z. (2008). *Normalized LDA for semi-supervised learning*. Paper presented at the IEEE International Conference on Automatic Face & Gesture Recognition.
- Harris, C. J. (1988). A combined corner and edge detector. *Proc Alvey Vision Conf*, 1988(3), 147-151.
- He, J., Zhang, Y., Li, X., & Wang, Y. (2011). *Bayesian classifiers for positive unlabeled learning*. Paper presented at the International Conference on Web-Age Information Management.
- Janai, J., Güney, F., Behl, A., & Geiger, A. (2017). Computer Vision for Autonomous Vehicles: Problems, Datasets and State-of-the-Art. *arXiv.org*.

- Jinhui He, Y. X., et al. (2015). Aerator state detection based on corner optical flow and SVM algorithm. *Computer Engineering & Science*, 37(8), 1566-1572.
- Jun, G., Aggarwal, J. K., & Gokmen, M. (2016). Tracking and Segmentation of Highway Vehicles in Cluttered and Crowded Scenes. 1-6.
- Kaewtrakulpong, P., & Bowden, R. (2002). An Improved Adaptive Background Mixture Model for Real-time Tracking with Shadow Detection. (September), 135-144.
- Kim, H. Y., & Chang, H. W. (2018). Forecasting the Volatility of Stock Price Index: A Hybrid Model Integrating LSTM with Multiple GARCH-Type Models. *Expert Systems with Applications*, 103.
- Krizhevsky, A., Sutskever, I., & Hinton, G. E. (2012). *ImageNet classification with deep convolutional neural networks*. Paper presented at the International Conference on Neural Information Processing Systems.
- Lee, J., Kim, S. J., & Lee, C. S. (2012). Effective scene change detection by using statistical analysis of optical flows. *Applied Mathematics & Information Sciences*, 6(1), 177S-183S.
- Li, W., Wu, X., Matsumoto, K., & Zhao, H. A. (2010). *Foreground detection based on optical flow and background subtract*. Paper presented at the International Conference on Communications, Circuits and Systems.
- Lu, C., & Tang, X. (2014). Surpassing Human-Level Face Verification Performance on LFW with GaussianFace. *Computer Science*.
- Lucas, B. D., & Kanade, T. (1981). *An iterative image registration technique with an application to stereo vision*. Paper presented at the International Joint Conference on Artificial Intelligence.
- Luxburg, U. v. (2007). A tutorial on spectral clustering. *Statistics and Computing*, 17(4), 395-416.
- Ma, C., Zhao, D., Wang, J., Chen, Y., & Li, Y. (2015). Intelligent monitoring system for aquaculture dissolved oxygen in pond based on wireless sensor network. *Transactions of the Chinese Society of Agricultural Engineering*, 31(7), 193-200.
- Mouy, X., Rountree, R., Juanes, F., & Dosso, S. E. (2018). Cataloging fish sounds in the wild using combined acoustic and video recordings. *The Journal of the Acoustical Society of America*, 143(5), EL333-EL339.
- Munther, A., Razif, R., Abualhaj, M., Anbar, M., & Nizam, S. (2016). A Preliminary Performance Evaluation of K-means, KNN and EM Unsupervised Machine Learning Methods for Network Flow Classification. *International Journal of Electrical & Computer Engineering*, 6(2), 778-784.
- Murugan, K. H. S., Jacintha, V., & Shifani, S. A. (2017). *Security system using raspberry Pi*. Paper presented at the International Conference on Science Technology Engineering & Management.
- OpenCV. (2017). Open Source Computer Vision. Available at: <<http://opencv.org/>>.
- Schmidt, M., Roux, N. L., & Bach, F. (2013). Minimizing finite sums with the stochastic average gradient. *Mathematical Programming*, 162(5), 1-30.
- Scikit-learn. (2017). Machine learning in Python. Available at: <<http://scikit-learn.org/>>.
- Shi, J. (1994). *Good Feature to Track*. Paper presented at the IEEE Conference on Computer Vision and Pattern Recognition.
- Shi, W., Caballero, J., Huszár, F., Totz, J., Aitken, A. P., Bishop, R., . . . Wang, Z. (2016). *Real-Time Single Image and Video Super-Resolution Using an Efficient Sub-Pixel Convolutional Neural Network*. Paper presented at the Computer Vision and Pattern Recognition.
- Sobral, A., & Vacavant, A. (2014). A comprehensive review of background subtraction algorithms evaluated with synthetic and real videos. *Computer Vision & Image Understanding*, 122(May 2014), 4-21.
- Solstorm, D., Oldham, T., Solstorm, F., Klebert, P., Stien, L. H., Vågseth, T., & Oppedal, F. (2018). Dissolved oxygen variability in a commercial sea-cage exposes farmed Atlantic salmon to growth limiting conditions. *Aquaculture*, 486, 122-129.
- Szczypiński, P. M., Klepaczko, A., & Zapotoczny, P. (2015). *Identifying barley varieties by computer vision*: Elsevier Science



Publishers B. V.

- Szekely, G. J., & Rizzo, M. L. (2005). Hierarchical Clustering via Joint Between-Within Distances: Extending Ward's Minimum Variance Method. *Journal of Classification*, 22(2), 151-183.
- Toyama, K., Krumm, J., Brumitt, B., & Meyers, B. (1999). *Wallflower: Principles and Practice of Background Maintenance*. Paper presented at the The Proceedings of the Seventh IEEE International Conference on Computer Vision.
- Wäldchen, J., & Mäder, P. (2018). Plant Species Identification Using Computer Vision Techniques: A Systematic Literature Review. *Archives of Computational Methods in Engineering*, 25(2), 1-37.
- Wan, P., Toudeshki, A., Tan, H., & Ehsani, R. (2018). A methodology for fresh tomato maturity detection using computer vision. *Computers & Electronics in Agriculture*, 146, 43-50.
- Wu, T. F., Lin, C. J., & Weng, R. C. (2004). Probability Estimates for Multi-class Classification by Pairwise Coupling. *Journal of Machine Learning Research*, 5(4), 975-1005.
- Zivkovic, Z. (2004). *Improved Adaptive Gaussian Mixture Model for Background Subtraction*. Paper presented at the Pattern Recognition, International Conference on.
- Zivkovic, Z., & Ferdinand, V. D. H. (2006). Efficient adaptive density estimation per image pixel for the task of background subtraction. *Pattern Recognition Letters*, 27(7), 773-780.